

Elasto-viscoplastic modeling of the consolidation of Sri Lankan peaty clay

Asiri Karunawardena¹, Fusao Oka*² and Sayuri Kimoto²

¹National Building Research Organization, 99/1, Jawatte Road, Colombo 5, Sri Lanka

²Department of Civil and Earth Resources Engineering, Kyoto University, Kyotodaigaku-katsura 4, Nishikyo-ku, Kyoto 615-8540, Japan

(Received December 6, 2010, Revised August 8, 2011, Accepted August 19, 2011)

Abstract: The consolidation behavior of Sri Lankan peaty clay is analyzed using an elasto-viscoplastic model. The model can describe the secondary compression behavior as a continuous process and it can also account for the effect of structural degradation on the consolidation analysis. The analysis takes into account all the main features involved in the process of peat consolidation, namely, finite strain, variable permeability, and the secondary compression. The material parameters required for the analysis and the procedures to evaluate them, using both standard laboratory and field tests, are explained. Initially, the model performance is assessed by comparing the predicted and the observed peat consolidation behavior under laboratory conditions. The results indicate that the model is capable of predicting the observed creep settlements and the effect of layer thickness on the settlement analysis of peaty clay. Then, the model is applied to predict the consolidation behavior of peaty clay under different field conditions. In this context, firstly, the one-dimensional field consolidation of peaty clay, brought about by the construction of compacted earth fill, is predicted. Then, the two-dimensional peat foundation response upon embankment loading is simulated. A good agreement is seen in the comparison of the predicted results with the field observations.

Keywords: amorphous type peat; finite strain; structural degradation; elasto-viscoplastic consolidation analysis.

1. Introduction

Peat deposits are found in many parts of Sri Lanka, including the capital city of Colombo and its suburbs. The process of urbanization, along with an increasing population and developments associated with this increase, has necessitated the utilization of these areas with peat deposits for new housing developments, industrial sites, and embankments for roads and highways. However, construction over peaty deposits always creates special problems due to the poor engineering properties of peaty soil. The major problem associated with the highly compressible nature of peat soil is the occurrence of excessive settlements. These settlements appear quickly and may continue for a long period of time due to the dominant creep behavior. In addition, low shear strength often causes stability problems in peat soils when they are subjected to external loading. Therefore, in

*Corresponding author, Professor, E-mail: oka.fusao.2s@kyoto-u.ac.jp

order to prevent differential settlements and subsequent potential failures, it is necessary to improve the strength and the stiffness properties of the natural peat deposits using appropriate ground-improvement techniques. It is important to understand and to quantify the consolidation response of peaty soils when employing such techniques and to predict the long-term settlements of structures supported by these soils.

Many extensive studies have been conducted on the consolidation behavior of peaty soils, by both empirical and experimental means, in the field and under laboratory conditions. An important conclusion which emerges from these studies is that there is a significant influence of secondary compression, rapid changes in permeability, and the resultant large strain on the consolidation analysis of peaty soils. The studies also reveal that the composition of natural deposits of peat may vary considerably among different sites, as do their mechanical properties (Berry and Poskitt 1972). Therefore, it is necessary to identify the type of peat under consideration. For example, the consolidation behavior of fibrous peat is different from that of amorphous granular peat, as amorphous granular peat has a lower organic content and a higher degree of decomposition than fibrous peat. Investigations reveal that peaty soils found in Sri Lanka are generally of the amorphous type and have a moisture content of 200%-800%, a void ratio of 2.0-8.0, an organic content of 20%-50%, a specific gravity of 1.5-2.2, and a pH value of less than 3.0 in their natural state.

In this paper, the consolidation behavior of amorphous peaty clay found in Sri Lanka is analyzed by considering all the main features involved in the process of peat consolidation, namely, secondary compression, finite strain, and changes in permeability. In addition to the above features, the effect of structural degradation on the peat consolidation process is investigated. Analyses are conducted using the elasto-viscoplastic model proposed by Kimoto and Oka (2005). The model can describe the secondary compression behavior as a continuous process and it can also account for the effect of structural degradation on the consolidation analysis. Initially, the applied constitutive model and the analysis methods to simulate the peat consolidation process are validated against the laboratory consolidation test results. Then, the model is applied to predict the consolidation behavior of peaty clay under different field conditions.

2. Elasto-viscoplastic model and analysis methods

The elasto-viscoplastic constitutive model proposed by Kimoto and Oka (2005) is based on Perzyna (1963) type viscoplastic theory and the Cambridge elasto-plastic theory (Roscoe *et al.* 1963) combined with empirical evidence. The most important assumption taken from the derivation of the model is that, "At the end of consolidation, the state of the clay does not reach the static equilibrium state but is in a non-equilibrium state" (Oka 2005). In the model, Terzaghi's effective stress is used in the following form

$$\sigma_{ij}' = \sigma_{ij} - u_w \delta_{ij} \quad (1)$$

where σ_{ij}' is the effective stress and u_w is the pore pressure. The total strain rate tensor consists of elastic strain rate tensor $\dot{\epsilon}_{ij}^e$ and viscoplastic strain rate tensor $\dot{\epsilon}_{ij}^{vp}$

$$\dot{\epsilon}_{ij} = \dot{\epsilon}_{ij}^e + \dot{\epsilon}_{ij}^{vp} \quad (2)$$

The elastic strain rate tensor is given by a generalized Hooke type of law, namely,

$$\dot{\varepsilon}_{ij}^e = \frac{1}{2G} \dot{S}_{ij} + \frac{\kappa}{3(1+e_0)\sigma'_m} \dot{\sigma}'_m \delta_{ij} \quad (3)$$

where S_{ij} is the deviatoric stress tensor, σ'_m is the mean effective stress, G is the elastic shear modulus, e_0 is the initial void ratio, κ is the swelling index, and the superimposed dot denotes the time differentiation.

In the model, the hardening rule is based on the overconsolidation (OC) boundary surface which delimitates the OC region ($f_b < 0$) from the normally consolidated (NC) region ($f_b \geq 0$) and is given as follows

$$f_b = \bar{\eta}^* + M_m^* \ln\left(\frac{\sigma'_m}{\sigma'_{mb}}\right) = 0 \quad (4)$$

In the above equation, $\bar{\eta}^*$ is the stress parameter that represents the anisotropic consolidation history defined by

$$\bar{\eta}^* = \sqrt{(\eta_{ij}^* - \eta_{ij(0)}^*)(\eta_{ij}^* - \eta_{ij(0)}^*)} \quad (5)$$

in which, for $\eta_{ij}^* = S_{ij}/\sigma'_m$, is the pressure normalized deviatoric stress tensor and $\eta_{ij(0)}^*$ is the value of η_{ij}^* before the deformation occurs (initial state). M_m^* is the value of $\sqrt{\eta_{ij}^* \eta_{ij}^*}$ when the volumetric strain increment changes from compression to swelling, and σ'_{mb} is the hardening parameter.

The viscoplastic strain rate tensor is calculated using the following flow rule which is based on Perzyna (1963) type viscoplastic theory

$$\dot{\varepsilon}_{ij}^{vp} = \gamma \langle \Phi_1(f_y) \rangle \frac{\partial f_b}{\partial \sigma'_{ij}} \quad (6)$$

where Φ_1 is a material function indicating the rate sensitivity, and f_y and f_p are the static yield and the potential functions, respectively, which are in the shape of the original Cam-clay type.

$$f_y = \bar{\eta}^* + \tilde{M}^* \ln\left(\frac{\sigma'_m}{\sigma'^{(s)}_{my}}\right) = 0 \quad (7)$$

$$f_p = \bar{\eta}^* + \tilde{M}^* \ln\left(\frac{\sigma'_m}{\sigma'_{mp}}\right) = 0 \quad (8)$$

In the above equations, $\sigma'^{(s)}_{my}$ denotes the mean effective stress in the static equilibrium state where stress may be reached after an infinite period of time. \tilde{M}^* is defined as

$$\tilde{M}^* = \begin{cases} M_m^* & : NC \text{ region} \\ \frac{\sqrt{\eta_{ij}^* \eta_{ij}^*}}{\ln(\sigma'_m / \sigma'_{mc})} & : OC \text{ region} \end{cases} \quad (9)$$

in which σ'_{mc} denotes the mean effective stress at the intersection of the OC boundary surface and the σ'_m axis. It can be expressed as

$$\sigma'_{mc} = \sigma'_{mb} \exp \frac{\sqrt{\eta_{ij(0)}^* \eta_{ij(0)}^*}}{M_m^*} \tag{10}$$

According to the above equation, σ'_{mc} equals σ'_{mb} in the case of isotropic consolidation.

Overconsolidation boundary surface f_b , static yield function f_y , and viscoplastic potential function f_p for $\eta_{ij}^* = 0$ are schematically described in the $\sigma'_m - \sqrt{S_{ij}S_{ij}}$ space for the NC region in Fig. 1.

Based on the experimental results of the constant strain-rate triaxial tests, material function Φ_1 , mentioned in Eq. (6), is defined as

$$\gamma \Phi_1(f_y) = C \sigma'_m \exp \left\{ m' \left(\bar{\eta}^* + \tilde{M}^* \ln \frac{\sigma'_m}{\sigma'_{mb}} \right) \right\} \tag{11}$$

where m' and C are viscoplastic parameters related to the coefficient of secondary consolidation and to the initial volumetric strain rate, respectively (Kimoto and Oka 2005).

Substituting Eq. (11) into Eq. (6) gives the viscoplastic strain rate as

$$\dot{\varepsilon}_{ij}^{vp} = C \sigma'_m \exp \left\{ m' \left(\bar{\eta}^* + \tilde{M}^* \ln \frac{\sigma'_m}{\sigma'_{mb}} \right) \right\} \frac{\partial f_b}{\partial \sigma'_{ij}} \tag{12}$$

2.1 Account of the effect of structural degradation

Originally, the changes in size of the σ'_{mb} surface were controlled only with respect to the viscoplastic volumetric strain as follows

$$\sigma'_{mb} = \sigma'_{mbi} \exp \left(\frac{1 + e_0}{\lambda - \kappa} \varepsilon_v^{vp} \right) \tag{13}$$

However, it has been observed that the behavior of natural soils is influenced by the degradation

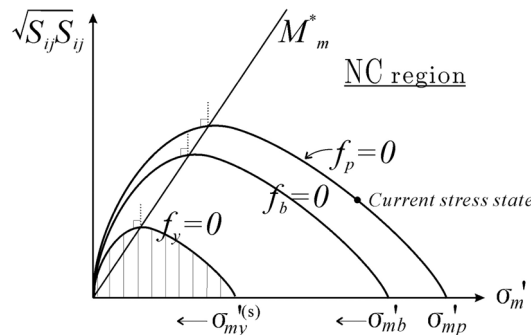


Fig. 1 OC boundary surface, static yield function, and viscoplastic potential function for normally consolidated clay (Kimoto and Oka 2005)

of the microstructure induced by the applied loads (Burland 1990). This effect has been incorporated into the model by introducing viscoplastic strain softening in addition to strain hardening with viscoplastic volumetric strain. This process was explained by Kimoto and Oka (2005) as follows

$$\sigma'_{mb} = \sigma'_{ma} \exp\left(\frac{1+e_0}{\lambda-\kappa} \varepsilon_v^{vp}\right) \quad (14)$$

$$\sigma'_{ma} = \sigma'_{maf} + (\sigma'_{mai} - \sigma'_{maf}) \exp(-\beta z) \quad (15)$$

where σ'_{ma} is assumed to decrease with an increasing viscoplastic strain, and σ'_{mai} and σ'_{maf} are the initial and the final values for σ'_{ma} , respectively. σ'_{mai} corresponds to the consolidation yield stress and σ'_{maf} is determined from the difference between the peak and the residual stress levels. Structural parameter β controls the rate of structural changes and z is an accumulation of the second invariant of the viscoplastic strain rate as follows

$$z = \int_0^t \dot{z} dt, \dot{z} = \sqrt{\dot{\varepsilon}_{ij}^{vp} \dot{\varepsilon}_{ij}^{vp}} \quad (16)$$

Due to this modification, the degradation of the soil structure leads to the shrinking of the overconsolidated (OC) boundary surface with the viscoplastic deformation.

The same procedure is adopted here by calculating $\sigma_{my}^{(s)}$ in the static yield function (Eq. (7)) and by taking the degradation effect into account. Accordingly, the decrease in $\sigma_{my}^{(s)}$ leads to the shrinking of the static yield function depending on the structural collapse.

2.2 Analysis methods to simulate peat consolidation

2.2.1 Changes in permeability and shear modulus

Changes in permeability coefficient k are taken into account using the following empirical relationship:

$$k = k_0 \exp(e - e_0) / C_k \quad (17)$$

where k_0 is the initial value for k at $e = e_0$ and C_k is the material parameter called the permeability change index.

Based on the laboratory test data, the elastic shear modulus is assumed to be proportional to $\sqrt{\sigma'_m}$ as

$$G = G_0 \sqrt{\frac{\sigma'_m}{\sigma'_{mo}}} \quad (18)$$

in which G_0 is the value for G when $\sigma'_m = \sigma'_{mo}$.

In the present analysis, we have not introduced the effect of Lode's angle on the constitutive model since we have not enough data to include the effect of Lode's angle on this Sri Lankan peaty clay. The simplest way is to assume Mohr-Coulomb criteria. But the in general Mohr-Coulomb criteria is not always true as has been reported by many researchers (Leroueil and Hight 2003). In addition, we have to consider the dependence of the strain direction on Lode's angle and the structural anisotropy. The Lode's angle dependency will be adopted in the future.

2.2.2 Relationship between viscoplastic parameter m' and C_α/C_c

Secondary compression is often more significant in peat soils than in inorganic clays, and therefore, it should be considered in the peat consolidation analysis. The strain rate parameter m' used in the model and the C_α/C_c concept proposed by Mesri *et al.* (1997) to predict the secondary consolidation were interrelated by Oka (2005) as follows

$$\alpha = \frac{\lambda - \kappa}{m'(1+e)M_m^*} \quad (19)$$

where α is the secondary compression rate given by $v^p (= \varepsilon_{kk}^{vp}) = \alpha \ln(t/t_0) + v_0^p$, λ is the compression index and κ is the swelling index given by the slope of the isotropic consolidation and swelling tests, respectively. M_m^* is the value of \hat{M}^* in normally consolidated region. In terms of the coefficient of secondary consolidation, $C_\alpha (= -de/d \log t)$, Eq. (19) can be expressed as

$$m' = \frac{C_c - C_s}{C_\alpha M_m^*} \quad (20)$$

where C_c is the compression index and C_s is the recompression index determined through the oedometer tests. Often in peat soils, and $C_s \approx 0.1C_c$, and $M_m^* \approx 1$ the viscoplastic parameter can be approximated as $m' = 0.9C_c/C_\alpha$.

This mathematically derived relationship between parameter m' and the C_c/C_α ratio of the soil was experimentally confirmed by Karunawardena (2007) by simultaneously conducting laboratory consolidation tests and triaxial tests on soft marine clay. Leroueil and Hight (2003) also experimentally verified the relationship between strain rate parameter m' and the C_α/C_c values for the soil reported by Mesri *et al.* (1995) and concluded that the two approaches used for describing the viscous behavior of soils during secondary consolidation are equivalent.

2.2.3 Formulation for finite deformation analysis

In the finite element formulations, which are based on the finite deformation theory, an updated Lagrangian method is adopted with the objective Jaumann rate of Cauchy stress for a weak form of the equilibrium equation (Oka *et al.* 2000, Oka *et al.* 2002, Kimoto *et al.* 2004, Higo *et al.* 2006).

Nominal stress rate tensor \dot{S}_{ij} , and the effective nominal stress tensor are given by

$$\dot{S}_{ij} = \dot{T}_{ij} + L_{kk}T_{ij} - T_{ij}L_{jk} \quad (21)$$

$$\dot{S}'_{ij} = \dot{T}'_{ij} + L_{kk}T'_{ij} - T'_{ik}L_{jk} \quad (22)$$

where T_{ij} is the Cauchy stress tensor, $T'_{ij} = T_{ij} - u_w \delta_{ij}$ is the effective Cauchy stress tensor, L_{ij} is the velocity gradient tensor, and the superimposed dot denotes the time differentiation.

The weak form of the equilibrium for the whole fluid-solid mixture is

$$\int_V \dot{S}_{ji,j} \delta v_i dV = 0 \quad (23)$$

where δv_i is the component of the virtual velocity vector.

For describing the motion of pore water, a Biot type of two-phase mixture theory is used in the analysis with a v_f (velocity) – u_w (pore pressure) formulation, i.e.

$$\frac{k}{\gamma_w} u_{w,ii} + D_{ii} = 0 \quad (24)$$

where γ_w is the unit weight of the pore fluid, k is the coefficient of permeability, and D_{ij} is the stretching tensor.

In the analysis, D_{ij} is used instead of $\dot{\varepsilon}_{ij}$ when writing the constitutive equations. The Jaumann rate of effective Cauchy stress tensor \hat{T}'_{ij} is used in the formulation. The Jaumann rate of effective Cauchy stress tensor \hat{T}'_{ij} is the objective tensor defined as

$$\hat{T}'_{ij} = \dot{T}'_{ij} - W_{ik} T'_{kj} + T'_{ik} W_{kj} \quad (25)$$

where W_{ij} is the spin tensor.

The relation between the Jaumann rate of Cauchy stress \hat{T}'_{ij} and the stretching tensor D_{ij} is obtained as

$$\hat{T}'_{ij} = C_{ijkl}^e D_{kl}^e = C_{ijkl}^e (D_{kl} - D_{kl}^{vp}) \quad (26)$$

in which C_{ijkl}^e is elastic tangential stiffness matrix, D_{ij}^e is the elastic stretching tensor, and D_{ij}^{vp} is the viscoplastic stretching tensor.

3. Finite element formulation based on finite deformation theory

In finite element formulations based on the finite deformation theory, the updated Lagrangian method is adopted with the objective Jaumann rate of Cauchy stress for a weak form of the equilibrium equation. Biot's two-phase mixture theory is used with a velocity-pore pressure formulation, and the pore water is defined at the four corner nodes of the element. A discretization of the equilibrium equation is presented followed by the continuity equation. In the finite element formulation, the tangent modulus method is used (Pierce *et al.* 1984). An eight-node quadrilateral element with a reduced Gaussian (2×2) integration is used to eliminate the shear locking and reduce the appearance of a spurious hourglass mode. On the other hand, the pore water pressure is defined at four corner nodes. A weak form of the continuity equation is integrated with a (2×2) full integration. Using this combination of the spatial integration scheme, the effective stresses, the pore water pressures, and the strain are all calculated at the same integration points for each element. The detailed procedures for discretizing the equilibrium equation, the continuity equation, and the governing equation, which combines the discretized form of both the equilibrium and the continuity equations used in the finite formulation based on the finite strain theory, are described in several papers e.g. Kimoto, Oka, Higo (2004), Higo, Oka., Kodaka and Kimoto (2006).

4. Determination of the model parameters

The material parameters required for the analysis are determined as follows:

For the compression index and the swelling index

$$\lambda = C_c / \ln 10 = 0.434 C_c \quad \text{and} \quad \kappa = C_s / \ln 10 = 0.434 C_s$$

where C_c and C_s are the compression and the recompression indices determined from the oedometer tests.

It has been observed that the coefficient of permeability calculated with Terzaghi's one-dimensional consolidation theory often underestimates the field value (Karunawardena and Kulatilaka 2003). In the present research, therefore, for the field analysis, the initial coefficient of permeability k_0 is based on the field permeability test results. Field permeability tests carried out on Sri Lankan peaty clay indicate that the in situ value for k_0 is in the order of 10^{-7} m/s. As related field data was not available, however, permeability change index C_k was deduced from the variations in permeability and the void ratio observed in the oedometer test.

Viscoplastic parameter m' is determined using the relationship mentioned in Eq. (26). It has been experienced that C_α , determined from long-term consolidation tests, can provide a more representative value in the case of peaty clay. The critical state parameter M_m^* is determined from the triaxial test results. The value of the earth pressure coefficient at rest, K_0 , used here, is based on the reported data by Edil and Dhowian (1981). They pointed out that K_0 , calculated from empirical correlations based on the measured value of the angle of internal friction of the soil (e.g. Jaky 1948), rarely agrees with the measured value of K_0 for peat, and thus, it has been suggested that the following values could be used for engineering purposes

$$\text{Fibrous peat} - K_0 = 0.3 \quad \text{Amorphous peat} - K_0 = 0.53$$

Compression yield stress σ'_{mbi} is related to the preconsolidation pressure determined through the oedometer tests. Viscoplastic parameter C , degradation parameter β , structural parameter σ'_{maf} , and initial shear modulus G_0 are determined by simulating the undrained triaxial tests. G_0 is first determined by the slope of stress-strain relation of triaxial tests and then improved by data-fitting method. Then the viscoplastic parameter C has been determined with no structural degradation effect, namely $\sigma'_{maf} = \sigma'_{mai}$. Finally, σ'_{maf} and β are determined by evaluating the magnitude of strain softening.

For this purpose, the results of the undrained triaxial tests conducted on peaty clay are numerically simulated using the elasto-viscoplastic model mentioned above. The results of the numerical simulation, which was performed to evaluate the above parameters for the analysis of the field consolidation behavior due to the construction of compacted earth fill on peaty clay, are shown in Figs. 2(a) and 2(b). The parameters used in the simulation are listed in Table 1. As shown in

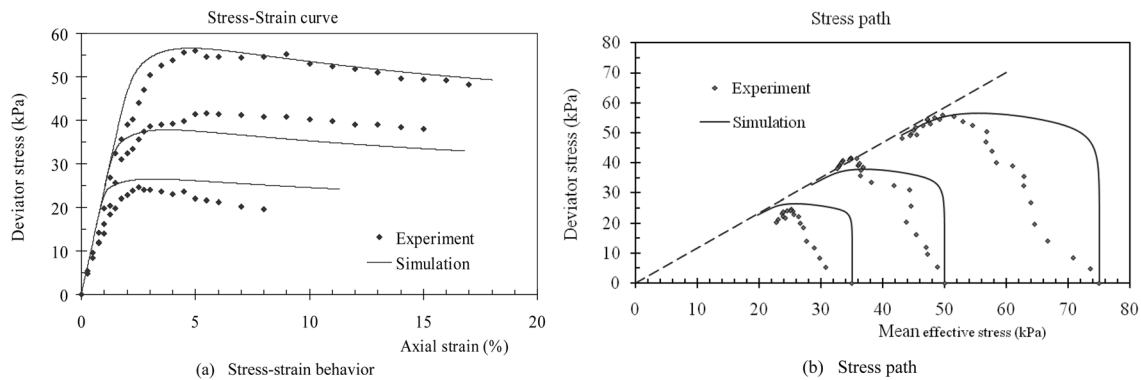


Fig. 2 Simulation of undrained triaxial test results

Table 1 Parameters used in the simulation of triaxial tests

Parameter	Value
Strain rate $\dot{\epsilon}$	0.11 (%/min)
Initial void ratio e_0	5.7, 5.4, 5.0
Initial elastic shear modulus [#] G_0	800 (kPa)
Compression index λ	1.7163
Swelling index κ	0.1151
Stress ratio at critical state M_m^*	0.95
Compression yield stress $\sigma'_{mbi}(\sigma'_{mai})$	35, 50, 75 (kPa)
Viscoplastic parameter m'	22
Viscoplastic parameter [#] C	1.0×10^{-10} (1/s)
Structural parameter [#] σ'_{mai}	0.7 σ'_{mbi} (kPa)
Structural parameter [#] β	5

[#]From the triaxial test stress-strain relationship

Fig. 2(b) the initial part of the stress path predicted by the simulation deviates quite a bit from that in the experimental results; however the prediction for the failure condition is satisfactory.

5. Model validation

This chapter demonstrates the capability of the constitutive model (Kimoto and Oka 2005) to capture the one-dimensional consolidation characteristics of peaty clay under laboratory conditions. For this purpose, data on the medium-scale consolidation model tests (275 mm in thickness and 203 mm in diameter) conducted on remolded peaty clay obtained from sites along the Colombo-Katunayaka Expressway (CKE) project, Sri Lanka reported by Kugan *et al.* (2004) was used. The normally consolidated behavior for load increments of 5-30 kPa (in steps of 5 kPa with 2-day time intervals) was predicted using the elasto-viscoplastic model and Terzaghi's one-dimensional model and compared with the measured strains. The material parameters used in the analysis are listed in Table 2; it should be noted that viscoplastic parameter C and structural parameters σ'_{maf} and β were assumed, while all the other parameters were based on the experimental results. In addition, the value of $\sigma'_{maf}/\sigma'_{mbi}$ is different between Tables 1. This is due to the different quality of the sample before testing.

As indicated in Fig. 3, the strain predicted by the elasto-viscoplastic model is higher than that of Terzaghi's model at the end of each load increment. Moreover, the figure shows that the development of strain ceases in Terzaghi's model after the dissipation of excess pore water pressure, whereas the development of strain progresses at a slow rate in the elasto-viscoplastic model, as observed in the experiments. This illustrates that the elasto-viscoplastic model can predict the observed creep behavior of peaty soil quite well, after the complete dissipation of excess pore water pressure as well as during the dissipation.

Table 2 Parameters for peaty clay¹⁾

Parameters for the elasto-viscoplastic model	
Parameter	Value
Initial void ratio e_0	5.80
Initial vertical effective stress $\sigma'_{22(0)}$	5.0 (kPa)
Coefficient of earth pressure at rest K_0	0.53
Coefficient of permeability k_0	4×10^{-8} (m/s)
Change in permeability index C_k	0.95
Initial shear modulus G_0	450 (kPa)
Compression index λ	0.8207
Swelling index κ	0.08946
Stress ratio at critical state M_m^*	0.98
Compression yield stress σ'_{mbi} (σ'_{mai})	3.5 (kPa)
Viscoplastic parameter m'	18
Viscoplastic parameter C	1.0×10^{-9} (1/s)
Structural parameter σ'_{maf}	3.0 (kPa)
Structural parameter β	5
Parameters for the Terzaghi model	
Coefficient of volume compressibility m_v	0.010 (kN/m ²)
Coefficient of consolidation c_v	5.0 (m ² /year)

¹⁾Peaty soil obtained in the Colombo-Katunayaka expressway project

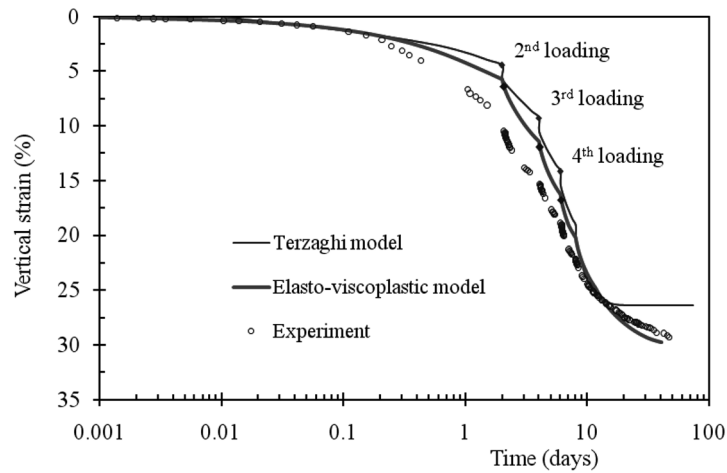


Fig. 3 Vertical strain-time profile

6. Prediction of settlements for specimens of different heights

The influence of specimen thickness on consolidation, which in turn plays an important role in predicting actual field consolidation behavior, has been addressed in several research works (e.g. Suklje 1969, Aboshi 1973, Ladd *et al.* 1977, Mesri and Choi 1985, Oka *et al.* 1986, Leroueil 1996,

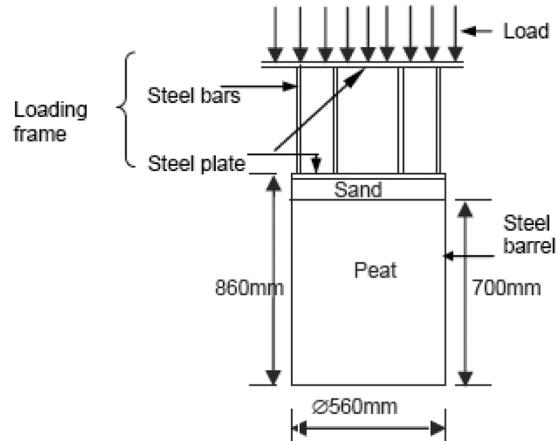


Fig. 4 Schematic diagram of the large-scale consolidation setup (Kugan *et al.* 2003)

Oka 2005). Aboshi (1973) experimentally observed that the initial strain rate for the thick sample is lower than that for the thin one. Oka *et al.* (1986) and Oka (2005) explained that the effect of sample thickness on a consolidation is mainly due to the rate-sensitive behavior of soil and that the effect can be successfully predicted by considering the difference in initial strain rates.

The model performance of the effect of sample thickness in the prediction of settlements is verified against the consolidation model tests on specimens with different heights reported by Kugan *et al.* (2003). Tests were conducted using the same remolded peaty clay that was used in the model validation described in the preceding section. Sample thicknesses were 700 mm, 275 mm, and 20 mm, and were referred to as large, medium, and small, respectively. A conventional oedometer was used here for the small scale tests, while a locally-fabricated apparatus with direct loading was adopted for the medium- and the large-scale models with diameters of 203 mm and 500 mm, respectively. The schematic diagram of the large-scale model is shown in Fig. 4. In the medium- and the large-scale models, drainage was allowed only at the top, while in the small-scale tests, drainage was allowed at both the top and the bottom. In all the tests, the load was applied in increments of 5 kPa, up to a final pressure amounting to 30 kPa.

The time duration of the load increment for the large-scale model was 2 days, while the duration of the other models was calculated assuming that the time required for the same degree of consolidation under a particular load increment is proportional to the square of the drainage length. After the load reached the final value of 30 kPa, samples were allowed to consolidate for a long period of time by maintaining the identical conditions; the settlements were monitored during that time.

Observed settlements for load increments of 5-30 kPa for different sample thicknesses were simulated by the model using the same material parameters, but considering the difference in the initial strain rates of the samples. The difference in initial strain rates was taken into account by viscoplastic parameter $C (= \dot{v}_{(0)}^p / M_m^*)$ which is related to the initial volumetric strain rate, $\dot{v}_{(0)}^p$, Adachi and Oka (1982), (Oka 2005). Consolidation under a load of 0-5 kPa was taken as the preparatory consolidation. Initially, a simulation was done for the medium-scale sample using the parameters listed in Table 2, except for parameter C . When parameter C was equal to $5.0 \times 10^{-9} \text{ s}^{-1}$, there was a good correlation between the model prediction and the experimental data. Then, a

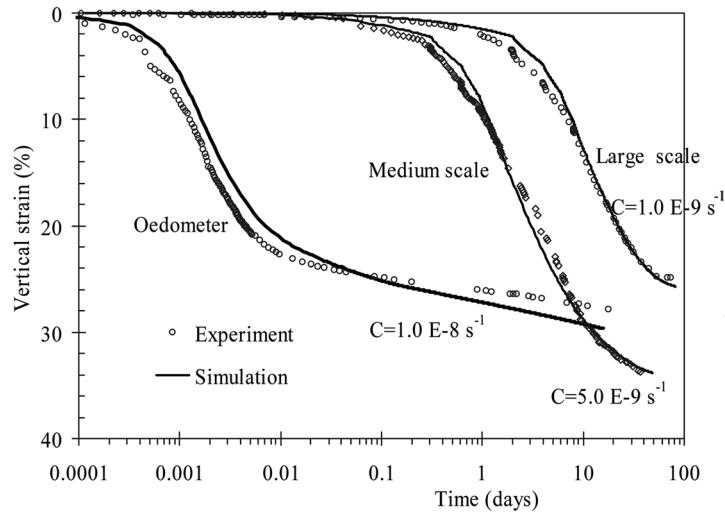


Fig. 5 Settlement predictions for different layer thicknesses

prediction was made for the large-scale model using the same parameters, except for the initial void ratio and parameter C . The experimental results indicate that the void ratio was 6.051 after the preparatory consolidation and parameter C was estimated based on the initial strain rate ratio between the large- and the medium-scale models. The results indicate that the average vertical strain rates for the medium- and the large-scale samples were $1.248 \times 10^{-4} \text{ %/s}$ and $2.589 \times 10^{-5} \text{ %/min}$, respectively, in the preparatory consolidation. According to these rates, and by approximating the strain at the end of the preparatory consolidation to its average strain rate, the ratio of the initial strain rates for medium- to large-scale samples was found to be 5 for the load increments considered in this analysis. In proportion to that, the C value for the large-scale model simulation became $1.0 \times 10^{-9} \text{ s}^{-1}$. Moreover, a prediction was made to simulate the observed strain of the small-scale model (oedometer) using the same material parameters. The test conditions e.g. the drainage and the height/diameter ratio, for the oedometer tests were different from those for the medium- and the large-scale tests, and therefore, a direct comparison of the initial strain rates is not logical. However, considering the fact that thin samples exhibit higher initial strain rates than thick samples, an analysis was carried out using a higher C value of $1.0 \times 10^{-8} \text{ s}^{-1}$. It should be noted that one-dimensional normally consolidated behavior was assumed in all of the above analyses.

Fig. 5 shows the predicted strain for each model with different samples thicknesses together with relevant experimental data. The predicted results show a reasonable agreement with the experimental data. It can be concluded, therefore, that the effect of sample thickness on the consolidation analysis of peaty clay, can be successfully predicted by the model considering the difference in initial strain rates among the samples.

7. Prediction of field consolidation behavior due to the construction of a compacted earth fill

A compacted earth fill was constructed in Fill Area 2 as part of the Madiwela Government project

Table 3 Parameters for the peaty clay¹⁾

Parameter	Value
Initial void ratio e_0	6.28
Initial vertical effective stress $\sigma'_{22(0)}$	10.25 [#] (kPa)
Coefficient of earth pressure at rest K_0	0.53
Coefficient of permeability k_0	1.5×10^{-7} (m/s)
Change in permeability index C_k	0.8
Initial shear modulus G_0	800 (kPa)
Compression index λ	1.7163
Swelling index κ	0.1151
Stress ratio at critical state M_m^*	0.95
Compression yield stress σ'_{mbi} (σ'_{mai})	12.5 [#] (kPa)
Viscoplastic parameter m'	22
Viscoplastic parameter C	1.0×10^{-10} (1/s)
Structural parameter σ'_{maf}	$0.7 \sigma'_{mbi}$ (kPa)
Structural parameter β	5

[#] at a depth of 2.5 m

¹⁾Peaty clay obtained in the Madiwela government project

in Sri Lanka in the year 2000. The peat was classified as being of the amorphous type, and the thickness of the peat layer was around 5 m. The fill was about 2.4 hectares and instruments were located around the center of the fill area. One-dimensional consolidation behavior was anticipated in the peat layer as the dimensions of the loaded area were significantly large in relation to the thickness of the compressible layer. A subsurface investigation revealed that the peat layer was underlain by a relatively rigid and permeable sandy silt layer. Under the same conditions, the peat layer is inelastic and much more compressible than the other layers, and therefore, only the peat layer was taken into consideration in the modeling. A finite element mesh with twenty-five elements was used to discretize the peat layer, and the size of each element was 0.2 m \times 0.2 m. The bottom boundary was assumed to be perfectly drained due to the existence of medium-dense to dense sandy silt layer underneath the peat layer. The investigation revealed that the compacted fill behaved as an impermeable layer, and therefore, the top boundary was assumed to be impermeable for simulating the field conditions. The material parameters used in the analysis were determined using the laboratory and the field tests carried out during the project period, following the procedure previously outlined and listed in Table 3.

The loading curve used in the analysis, which shows the construction sequence of the fill, is presented in Fig. 6 together with the excess pore water pressure-time profile. The stress in the loading curve was calculated as the product of the fill thickness and the total unit weight of the fill based on the field records. Field density test results indicate that the total unit weight of the fill varied from 15 kN/m³ to 18 kN/m³.

In the analysis, both finite strain (FS) and infinitesimal strain (IS) computations were made to explore how these two approaches describe the observed behaviors. In the finite element analysis considering FS, the method outlined previously was adopted, while in the analysis considering IS, a four-node quadrilateral element with a reduced Gaussian two-point integration was used for the

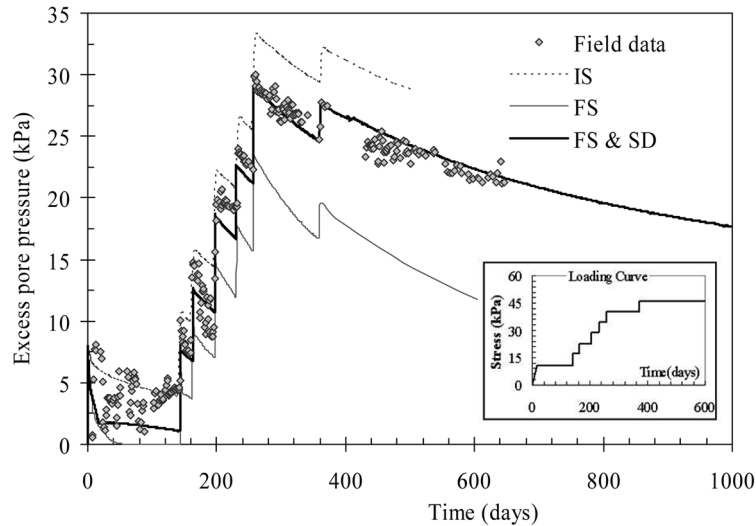


Fig. 6 Excess pore water pressure-time profile

displacement, and the pore water pressure was defined at the center of each element (Oka *et al.* 1986, Kimoto and Oka 2005). In order to investigate the degradation effect on the consolidation behavior of peaty clay, a separate analysis was carried out by considering finite strain together with the degradation effect; the corresponding analyses are referred to as FS & SD.

7.1 Excess pore pressure and settlement predictions

The predicted and the observed excess pore water pressures in the middle of the peat layer; 2.5 m in depth, are presented in Fig. 6. It indicates that the field pore water pressure reached around 30 kPa at the completion of the fill due to a load of 46 kPa. After the completion of the fill, the quantity of dissipated excess pore water pressure was only about 10 kPa during the following year.

When this behavior is compared with the predicted behavior, it shows that the prediction made by the IS theory overestimates the excess pore water pressure. In contrast, the FS theory underestimates the prediction when it is compared with the observed field data. Only the predictions made by FS & SD agree remarkably with the observed field behavior. The above results indicate that when predicting the excess pore water pressure behavior in highly compressible materials like peat, it is necessary to consider the changes in geometry ;decrease in soil layer height, in order to account for the correct drainage path. Moreover, it is essential to consider the effect of structural degradation along with the finite strain in order to simulate the stagnated pore pressure observed after the construction.

A comparison between the predicted and the actual settlements just underneath the fill is presented in Fig. 7. Field settlement data indicates that the settlement advances even though no significant dissipation of the excess pore water pressure actually takes place in the field. This unusual phenomenon, namely, the settlement advancing with stagnation of the excess pore water pressure after the end of loading, has been observed in many construction works over soft deposits around the world. Many researchers suggest that this behavior occurs due to the effect of the structural degradation of the compressible layer (e.g. Mitchell 1981). Kimoto and Oka (2005)

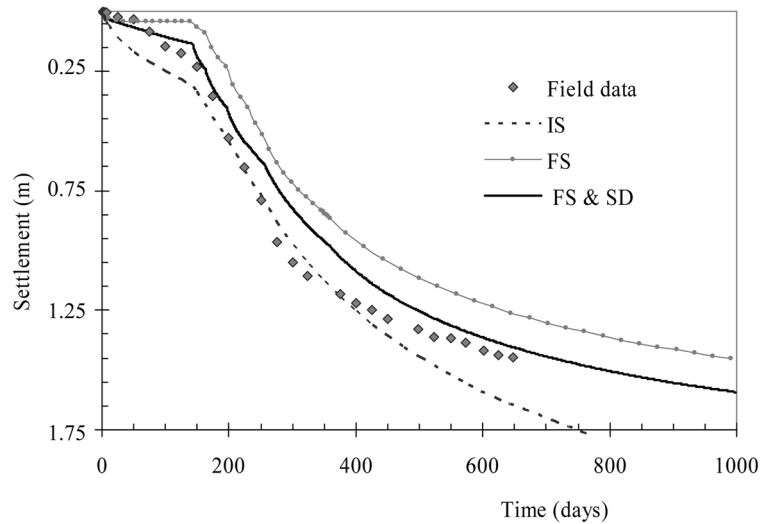


Fig. 7 Settlement-time profile just beneath the fill

simulated this behavior numerically by considering the degradation effect in the consolidation process. A comparison shows that, as expected, the predicted settlement assuming IS gives a higher value than that assuming FS, and in this case, the difference is more significant due to the resultant large strain of around 20% in the field. Predictions made by the IS theory overestimate the field settlements, whereas those made by the FS theory show a qualitative agreement with the observed data, even though it underestimates the actual settlement quantitatively. Similar to the pore water pressure predictions, FS & SD show better qualitative and quantitative agreements with the observed field data for the parameters used in this analysis.

The performance of the model which considers the finite strain with the effect of structural degradation can be clearly seen in this analysis. As shown in the figures, the predicted settlement for the case with the degradation effect advances faster than that for the case without the degradation effect, but the difference in the advance in settlement between the two is not so significant. On the other hand, a big difference is clearly seen in the prediction of the excess pore water pressure in the peat layer. Although only a slight difference exists for the advance in settlement between the two cases, the decreasing rate of the excess pore water pressure for the case which considers the degradation effect is small even after the end of loading, while the excess pore water pressure for the case which does not consider the degradation effect starts to dissipate significantly after the completion of loading. The average dissipation rate for FS (0.0375 kPa/day) is 1.875 time larger than that (0.02 kPa/day) for FS + SD. This indicates that the effect of structural degradation plays an important role when analyzing the consolidation behavior of natural soil deposits. The structural degradation leads to the stagnation or generation of the excess pore water pressure and the corresponding lower settlement rate during the consolidation, and manifests strain softening in the shearing test. The initial anisotropy is another feature of the peaty soil but this point has to be studied more in detail in the future.

8. Simulation of field behavior due to embankment construction

Herein, the simulation of the field behavior of peaty clay due to embankment construction is presented. The trial embankment at Ch.11 + 950 in the Colombo-Katunayaka Expressway (CKE) project, Sri Lanka was constructed using preloading with a surcharge as the ground-improvement technique. The embankment has a height of 5.9 m and 1:2 side slopes with a surcharge of 0.94 m fill and a crest width of 13.6 m. Ketheeswaravenayagam (2006) reported that there exists at the surface a highly compressible peat layer, 1 m in thickness, followed by a very loose fine sand layer, up to 2 m in depth. Below that, a soft silty sand/clay layer is encountered. It is 4.5 m in thickness and contains pockets of peat. The assumed geotechnical profile considered in the analysis is shown in

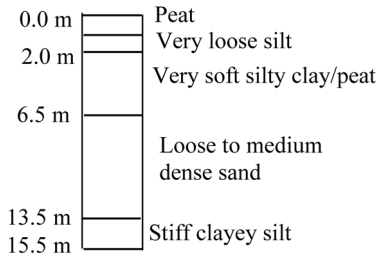


Fig. 8 Subsurface profile used in the analysis

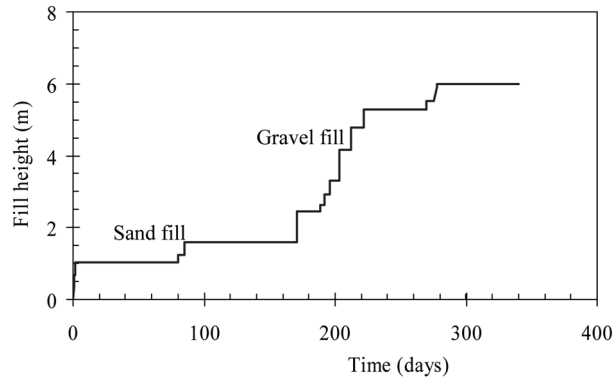


Fig. 9 Loading profile

Table 4 Parameters for soft soil layers

Parameter	Value (Peaty clay) ¹⁾	Value (silt layer) ²⁾
Initial void ratio e_0	6.5	1.8
Initial vertical effective stress $\sigma'_{22(0)}$	9.0 (kPa)	12.0 (kPa)
Coefficient of earth pressure at rest K_0	0.53	0.5
Coefficient of permeability k_0	8.0×10^{-7} (m/s)	5.5×10^{-7} (m/s)
Change in permeability index C_k	1.0	0.9
Initial elastic shear modulus G_0	800 (kPa)	1000 (kPa)
Compression index λ	1.505	0.203
Swelling index κ	0.096	0.011
Stress ratio at critical state M_m^*	0.95	1.1
Compression yield stress σ'_{mbi} (σ'_{mai})	9.0 (kPa)	12.0 (kPa)
Viscoplastic parameter m'	22	30
Viscoplastic parameter C	1.0×10^{-9} (1/s)	1.0×10^{-10} (1/s)
Structural parameter σ'_{maf}	$0.7 \sigma'_{mbi}$ (kPa)	$0.7 \sigma'_{mbi}$ (kPa)
Structural parameter β	5.0	5.0

¹⁾Peaty clay obtained in the Colombo-Katunayaka expressway project; peaty soil layer between 0-1 m and soft silty clay and peat (2-6.5 m)

²⁾Loose silt obtained in the Colombo-Katunayaka expressway project; Loose silt layer between 1-2 m

Fig. 8. A loading curve that reflects the construction history of the embankment is shown in Fig. 9.

A two-dimensional elasto-viscoplastic finite element analysis was performed to simulate the observed field behavior by considering the finite deformation theory together with the effect of structural degradation. In the modeling, the behavior of the peat, the very loose sand, the soft silty sand/clay, and the stiff clay was assumed to be elasto-viscoplastic, while the behavior of loose to medium dense sand and the stiff clay layer was assumed to be elastic. The analysis was carried out using the parameters listed Tables 4 and 5. The values of the unit weight of layers are listed in Table 6. The grass mat existing on the original ground surface, that gave additional strength to the subsoil, was modeled as a thin elastic element. In the analysis, drainage was permitted only at the top boundary and the excess pore water pressure was initially assumed to be zero in the subsoil. At the vertical boundaries, the displacement was constrained horizontally but allowed to move vertically. At the bottom boundary, movements in both directions were restrained. The embankment loading was simulated by applying incremental vertical loads according to the actual construction sequence of the embankments. For this purpose, total unit weights of 20 kN/m³ and 17.4 kN/m³ were assumed for the initial sand mat and the subsequent gravel fill used in the construction, respectively.

The material parameters required for the analysis were determined based on the data reported by Ketheeswaravenayagam (2006) and other reported literature relevant to amorphous peaty clay. The determined model parameters for the peaty clay are listed in Table 4. It should be noted that the very soft silty clay/peat layer at a depth of 2 to 6.5m indicated in the subsurface profile was modeled in the analysis with the same properties for the peaty clay by considering the observed large settlement. This assumption is further confirmed by the borehole data taken at Ch.11 + 900.

The final height of the embankment was about 6 m shown in Fig. 9, and therefore, the expected

Table 5 Parameters used for the layers at 6.5-13.5 m depth

Parameter	Value (Depth 6.5-10 m)	Value (Depth 10 m-13.5 m)
Initial void ratio e_0	1.8	1.8
Initial vertical effective stress $\sigma'_{22(0)}$	37.0 (kPa)	61.0 (kPa)
Coefficient of earth pressure at rest K_0	0.5	0.5
Coefficient of permeability $k_x = k_y$	5.5×10^{-7} (m/s)	5.5×10^{-7} (m/s)
Change in permeability index C_k	0.9	0.9
Initial Young's modulus E	8500 (kPa)	12000 (kPa)
Poisson ratio ν	0.3	0.3

Table 6 Unit weight of soils for two-dimensional analysis

Depth (m)	Soil type	Saturated unit weight (kN/m ³)
0-1	Peat	11.0
1-2	Very loose silt	13.5
2-6.5	Silty clay/peat	13.0
6.5-9.5	Loose to medium dense sand	16.5
9.5-13.5	Loose to medium dense sand	17.0
13.5-15.5	Stiff clayey soil	17.0

increase in vertical stress under the embankment foundation was more than 100 kPa. The embankment was constructed in stages and the total construction period was fairly long, as shown in Fig. 9. Thus, by considering the reduction in compressibility parameters at higher stress levels associated with the peat consolidation process (Hobbs 1986), as well as the highly nonlinear nature of the $e - \log \sigma'_v$ curve in peaty soil, the use of variable compressibility parameters corresponding to a particular void ratio and effective vertical stress level is found to be more realistic with the field conditions. However, for this embankment analysis, there were not enough consolidation test results to determine the compressibility parameters for each stress level. Therefore, these parameters were assumed to

$$\lambda = \lambda_i \left(\frac{1+e}{1+e_0} \right) \quad (27)$$

$$\kappa = \kappa_i \left(\frac{1+e}{1+e_0} \right) \quad (28)$$

where λ_i and κ_i are the initial compression index and swelling index shown in Table 4.

For the distribution of the initial void ratio, we have used the same value at a depth of 1m for the whole depth of peat due to the lack of data. Material parameters for very loose silt layer found at a depth of 1 m-2 m are also listed in Table 4.

8.1 Prediction of deformation and excess pore water pressure

Fig. 10 shows the predicted and the measured settlements just below the center of the embankments. For the initial discrepancy indicated in the predicted and the observed results under the center, there is no definite reason for that. Probably, this might be due to the measurement problem. In the development of settlement under an embankment at ground level, it is usually taken for granted that the maximum settlement always occurs at the center. While this is true for most soft

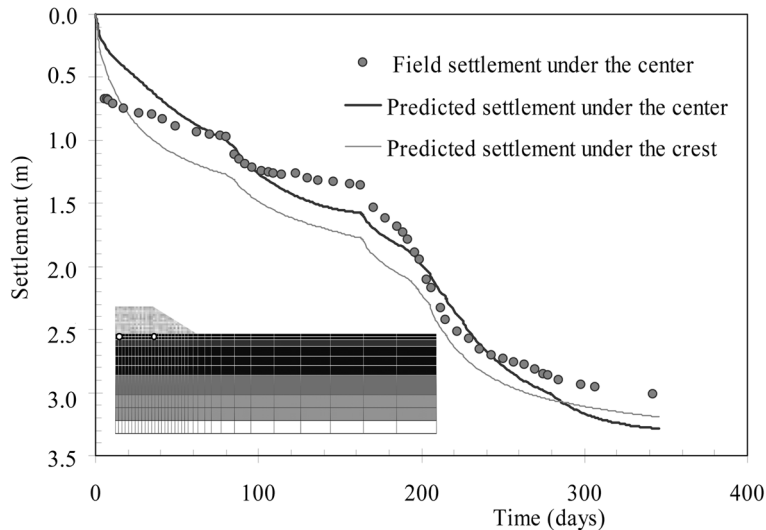


Fig. 10 Comparison between prediction and measurement

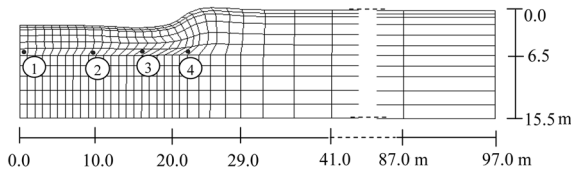


Fig. 11 Deformed mesh after 215 days

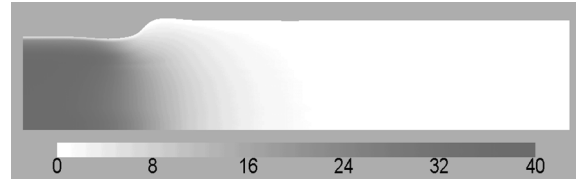


Fig. 12 Variation in excess pore pressure (kPa) during construction (after 215 days)

soil foundations of average dimensions, the calculated results here indicate that the predicted settlements under the shoulder area of the embankment is greater than that of central area during the construction period. The predicted settlement under the crest area (12.5 m away from the center) is shown in Fig. 10. The deformed geometry of the embankment foundation after 215 days is presented in Fig. 11; it also confirms that the maximum settlement was not predicted at the center during the construction period. If an embankment is extremely wide, compared to its height, the stress condition in the central area of the foundation is approximately one dimensional and the condition in the shoulder area is two dimensional. The higher settlement that was predicted under the shoulder area of the embankment foundation was possibly due to the result of local shear-induced displacements. However, the maximum excess pore water pressure dissipation was always predicted around the center area and the distribution of excess pore water pressure under the embankment after 250 days (during the construction of the embankment) is shown in Fig. 12. In addition to excessive settlements, the embankments constructed on peaty clays are subjected to large outward lateral displacements. As indicated in Fig. 11, a large lateral deformation occurred beneath the toe of the embankment.

8.2 Discussion of the stability

The above-mentioned lateral deformation is mainly caused by the shear stress induced by the

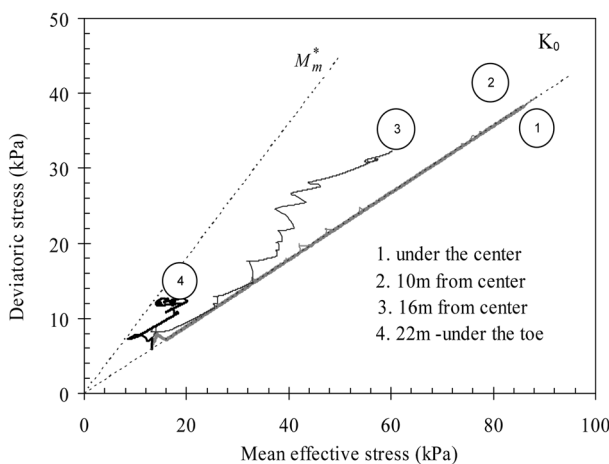


Fig. 13 Stress paths under the embankment (No. in the figure corresponds to that in Fig. 11)



Fig. 14 Variation in viscoplastic shear strain during construction (after 215 days)

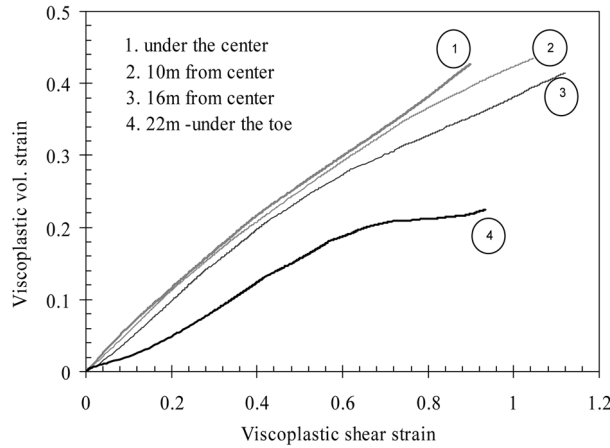


Fig. 15 Variations in viscoplastic volumetric strain vs. viscoplastic shear strain (No. in the figure corresponds to that in Fig. 11)

embankment load, and if the shear stress is large enough, it will cause shear failure within the subsoil. Therefore, the stability of an embankment on peaty soil is very important due to the soft consistency of peat as well as other soft soils. With regard to this, the effective stress paths were analyzed, followed by the different soil elements as indicated in Fig. 11, under the embankments.

As shown in Fig. 13, the stress paths of elements under the center area move along the K_0 path, whereas the stress paths of elements under the toe area rise towards the critical state line. This indicates that the toe area is more prone to inelastic instability, i.e. development of large inelastic shear deformation, than the center region under this embankment geometry. This is further illustrated by the distribution of the accumulated viscoplastic shear strain ε_q^{vp} of the embankment foundation and the viscoplastic volumetric strain ε_v^{vp} vs. shear strain ε_q^{vp} graphs, as shown in Figs. 14 and 15, respectively. In Fig. 14, it can be clearly seen that localized large strain develops underneath the toe region of the embankment. Fig. 15 indicates that $d\varepsilon_v^{vp}/d\varepsilon_q^{vp}$ of the element under the toe area approaches zero during some stages of the embankment construction. Here, $\varepsilon_v^{vp} = \int (de_{ij}^{vp} de_{ij}^{vp})^{1/2}$ where de_{ij}^{vp} is the viscoplastic shear strain increment tensor.

9. Conclusions

This paper presented a study on the numerical simulation of the consolidation behavior of peaty clay found in Sri Lanka using the elasto-viscoplastic model (Kimoto and Oka 2005). Analyses were performed considering all the main features involved in the peat consolidation process, namely, finite strain, variable permeability and compressibility, and the effect of secondary compression which is assumed as a continuous process. In addition to these main features, the effect of structural degradation on the consolidation was considered by introducing viscoplastic strain softening in addition to strain hardening with viscoplastic volumetric strain. In the model, the secondary compression was taken into account by viscoplastic parameter m' , which is related to the C_α/C_c ratio of the soil. The value of permeability was varied with the void ratio throughout the consolidation process. Finite element analyses were carried out considering finite deformation using

the updated Lagrangian method.

The material parameters were obtained using the available laboratory and field test results, and empirical correlations were used in cases where there was a lack of test data. The conclusions obtained from this study are as follows:

- (1) The model assumption of the occurrence of creep (or secondary) settlement as a continuous process agrees well with the observed consolidation behavior under laboratory conditions. The effect of using the results of laboratory tests on a thin soil specimen to predict the development of strain with time for thick soil layers in the field can be successfully taken into consideration with the model by keeping in mind the difference in initial strain rates.
- (2) The simulation of the field consolidation behavior of peaty clay, due to the construction of compacted earth fill, reveals that the finite deformation theory is more representative than the infinitesimal strain theory for the peat consolidation process. The effect of structural degradation has significance in the prediction of both the observed settlement and the stagnated excess pore pressure observed in the field. The analysis indicates that the consideration of the effect of structural degradation on the consolidation analysis provides realistic in situ behavior for natural soil deposits.
- (3) The embankment analysis of natural peaty clay indicates that the model and the analysis method are applicable to reproduce both the deformation and the stability aspects of foundations including peaty soft clays.

Acknowledgments

The authors are grateful to the Road Development Authority, University of Moratuwa, and to the National Building Research Organization of Sri Lanka for providing the necessary data for this research work.

References

- Aboshi, H. (1973), "An experimental investigation on the similitude consolidation of clay including secondary creep settlement", *Proc. of 8th ICSMFE*, Moscow, **4**(3), 88.
- Adachi, T. and Oka, F. (1982) "Constitutive equations for normally consolidated clay based on elasto-viscoplasticity", *Soils Found.*, **22**(4), 55-70.
- Berry, P.L. and Poskitt, T.J. (1972), "The consolidation of peat", *Geotechnique*, **22**(1), 27-52.
- Burland, J.B. (1990), "On the compressibility and shear strength of natural clays", *Geotechnique*, **40**(3), 329-378.
- Edil, T.B. and Dhowian, A.W. (1981), "At-rest lateral pressure of peat soils", *J. Geotech. Eng. - ASCE*, **107**(GT2), 201-217.
- Higo, Y., Oka, F., Kodaka, T. and Kimoto, S. (2006), "Three-dimensional strain localization of water-saturated clay and numerical simulation using an elasto-viscoplastic model", *Philos. Mag.*, **86**(21-22), 3205-3240.
- Hobbs, N.B. (1986), "Mire morphology and the properties and behavior of some British and foreign peats", *Q. J. Eng. Geol. Hydroge.*, **19**, 7-80.
- Jaky, J. (1948), "State of stress at great depth", *Proc. of 2nd ICSMFE*, **1**, 103-107.
- Karunawardena, W.A. (2007), *Consolidation analysis of Sri Lankan peaty clay using elasto-viscoplastic theory*, Ph.D. Thesis, Kyoto University, Japan.
- Karunawardena, W.A. and Kulatilaka, S.A.S. (2003), "Field monitoring of a fill on peaty clay and its modeling", *Proc. of 12th Asian Regional Conf. on Soil Mechanics & Geotechnical Eng.*, Singapore, 4-8, August 2003,

- Lung *et al.* eds., World Scientific Publishing Co. **1**, 159-162.
- Ketheeswaravenayagam, R. (2006), *Finite element modeling of highway embankments over soft sub soil conditions*, Master Thesis, University of Moratuwa, Sri Lanka.
- Kimoto, S. and Oka, F. (2005), "An elasto-viscoplastic model for clay considering destructuration and consolidation analysis of unstable behavior", *Soils Found.*, **45**(2), 29-42.
- Kimoto, S., Oka, F. and Higo, Y. (2004), "Strain localization analysis of elasto-viscoplastic soil considering structural degradation", *Comput. Method. Appl. M.*, **193**, 2845-2866.
- Kugan, R., Puswewala, U.G.A., Kulathilaka, S.A.S. and Peiris, T.A. (2003), "Peaty clay improvement with prefabricated vertical drains", *Proc. of Engineering Research Unit*, University of Moratuwa, Sri Lanka.
- Kugan, R., Puswewala, U.G.A., Kulathilaka, S.A.S. and Peiris, T.A. (2004), "Consolidation testing of peaty clay", *Proc. of Engineering Research Unit*, University of Moratuwa, Sri Lanka.
- Ladd, C.C., Foott, R., Ishihara, K., Schlosser, F. and Poulos, H.G. (1977), "Stress-deformation and strength characteristics", *Proc. of 9th ICSMFE*, Tokyo, **2**, 421-494.
- Leroueil, S. and Hight, D.W. (2003), *Behavior and properties of natural soils and soft rocks*, Characterization and Engineering Properties of Natural Soils, Tan *et al.* eds., 29-254.
- Leroueil, S. (1996), "Compressibility of clays: Fundamental and practical aspects", *J. Geotech. Eng. Div. - ASCE*, **122**(7), 534-543.
- Mesri, G., Shahien, M. and Feng, T.W. (1995), "Compressibility parameters during primary consolidation", *Proc. Int. Symp. on Compression and Consolidation of Clay soils- IS - Hiroshima's 95*, Japan, H. Yoshikuni and O. Kusakabe eds., Balkema, Rotterdam, **2**, 1021-1037.
- Mesri, G. and Choi, Y.K. (1985), "The uniqueness of the end-of-primary (EOP) void ratio-effective stress relationship", *Proc. 11th ICSMFE*, San Francisco, 2587-2590.
- Mesri, G., Stark, T.D., Ajlouni, M.A. and Chen, C.S. (1997), "Secondary compression of peat with or without surcharging", *J. Geotech. Eng. - ASCE*, **123**(5), 411-421.
- Mitchell, J.K. (1981), "Soil improvement-state of the art report", *Proc. of 10th ICSMFE*, Stockholm, **4**, 509-565.
- Oka, F., Adachi, T. and Okano, Y. (1986), "Two-dimensional consolidation analysis using an elasto-viscoplastic constitutive equation", *Int. J. Numer. Anal. Method. Geomech.*, **10**, 1-16.
- Oka, F. (2005), "Computational modeling of large deformations and the failure of geomaterials, theme lecture", *Proc. of 16th ICSMFE*, Osaka, **1**, 47-95.
- Oka, F., Higo, Y. and Kimoto, S. (2002), "Effect of dilatancy on the strain localization of water-saturated elasto-viscoplastic soil", *Int. J. Solids Struct.*, **39**, 3625-3647.
- Oka, F., Yashima, A., Sawada, K. and Aifantis, E.C. (2000), "Instability of gradient-dependent elastoviscoplastic model for clay and strain localization", *Comput. Method. Appl. M.*, **183**, 67-86.
- Perzyna, P. (1963), "The constitutive equations for work-hardening and rate sensitive plastic material", *Proc. Vibrational Problems*, Warsaw, **4**(3), 281-290.
- Pierce, D., Shih, C.F. and Needleman, A. (1984), "A tangent modulus method for rate dependent solids", *Comput. Struct.*, **18**(5), 875-887.
- Roscoe, K.H., Schofield, A.N. and Thurairajah, A. (1963), "Yielding of clays in state wetter than critical", *Geotechnique*, **13**(3), 221-240.
- Suklje, L. (1969), *Rheological aspects of soil mechanics*, Wiley-Interscience, A division of John Wiley & Sons Ltd.